

LETTER TO THE EDITOR

First simultaneous multi-wavelength observations of the black hole candidate IGR J17091–3624

ATCA, INTEGRAL, Swift, and RXTE views of the 2011 outburst

J. Rodriguez¹, S. Corbel¹, I. Caballero¹, J.A. Tomsick², T. Tzioumis³, A. Paizis⁴, M. Cadolle Bel⁵, and E. Kuulkers⁵

¹ Laboratoire AIM, CEA/IRFU - CNRS/INSU - Université Paris Diderot, CEA DSM/IRFU/SAP, F-91191 Gif-sur-Yvette, France

² Space Sciences Laboratory, 7 Gauss Way, University of California, Berkeley, CA 94720-7450, USA

³ Australia Telescope National Facility, CSIRO, P.O. Box 76, Epping NSW 1710, Australia

⁴ Istituto Nazionale di Astrofisica, INAF-IASF, Via Bassini 15, 20133 Milano, Italy

⁵ ESAC, ISOC, Villañueva de la Cañada, Madrid, Spain

ABSTRACT

We present the results of the first four (quasi-)simultaneous radio (*ATCA*), X-ray (*Swift*, *RXTE*), and γ -ray (*INTEGRAL*) observations of the black hole candidate IGR J17091–3624, performed in February and March 2011. The X-ray analysis shows that the source was in the hard state, and then it transitioned to a soft intermediate state. We study the correlated radio/X-ray behaviour of this source for the first time. The radio counterpart to IGR J17091–3624 was detected during all four observations with the *ATCA*. In the hard state, the radio spectrum is typical of optically thick synchrotron emission from a self-absorbed compact jet. In the soft intermediate state, the detection of optically thin synchrotron emission is probably due to a discrete ejection event associated with the state transition. The position of IGR J17091–3624 in the radio versus X-ray luminosity diagram (aka fundamental plane) is compatible with that of the other black hole sources for distances greater than 11 kpc. IGR J17091–3624 also appears as a new member of the few sources that show a strong quenching of radio emission after the state transition. Using the estimated luminosity at the spectral transition from the hard state, and for a typical mass of $10M_{\odot}$, we estimate a distance to the source between ~ 11 and ~ 17 kpc, compatible with the radio behaviour of the source.

Key words. Accretion, accretion discs; X-rays: binaries; Radio continuum: stars, Stars: individuals: IGR J17091–3624, GRS 1915+105, GX 339–4, H1743–322

1. Introduction

Most of the ~ 40 Galactic black hole binaries (BHB) are transient sources that are detected in X-rays during bright, months-to-year long outbursts. During this period, their luminosity varies by several orders of magnitude. At the same time, the broad band (~ 0.1 – 200 keV) X-ray spectra show pivoting from the canonical hard state (HS) to the canonical soft state (SS), through intermediate flavours of these last two. These states also have clear signatures in the temporal domain (0.1–1000 Hz), with the appearance of different types (dubbed A, B, C) of quasi periodic oscillations (QPO) in the HS, hard intermediate (HIMS), and soft intermediate (SIMS) states (e.g. Remillard & McClintock 2006; Homan et al. 2005; Remillard et al. 2002).

BHBs are also known to produce strong radio emission, either from a powerful compact jet in the HS or from relativistic discrete ejections at the transition from the HIMS to the SIMS (e.g., Fender 2006). In the HS, a strong correlation between the X-ray and radio luminosity has been found by Corbel et al. (2003) who point out a very strong coupling between the compact jets and the inner accretion flow. For Cyg X-1, this jet has been detected above ~ 500 keV (Laurent et al. 2011). The $L_{\text{Radio}}=L_{\text{X}}^{0.6}$ relation between the radio and X-ray luminosities is thought to be universal (aka the “standard” pattern or GX 339–4 like behaviour), although it is based on only eight

Galactic sources (among which GX 339–4 and Cyg X-1 show a large quenching of the radio emission in the SS; Corbel et al. 2003; Fender et al. 2010). Seven sources have recently been shown to define a new track in the radio versus X-ray luminosity diagram by following the relation $L_{\text{Radio}}=L_{\text{X}}^{1.4}$ (hereafter the H1743–322 like behaviour; Fender et al. 2010; Coriat et al. 2011). The total number of BHBs simultaneously followed in a multi-wavelength way is, however, still low. It is, thus, not clear which of the two types of behaviour (GX 339–4 or H1743–322-like) is the most common, or what leads to these differences. Multi-wavelength observations of any new active target, over the widest possible range of luminosities are, therefore, important for better understanding the jet behaviour and assessing the links between the accretion and ejection processes. To this end, we conducted Australian Telescope Compact Array (*ATCA*) and Rossi X-ray Timing Explorer (*RXTE*) observations as soon as IGR J17091–3624 was seen to enter a new outburst in 2011.

IGR J17091–3624 was discovered with the International Gamma-Ray Astrophysics Laboratory (*INTEGRAL*) on April 14, 2003 while entering outburst (Kuulkers et al. 2003). Observations with other facilities (e.g. *RXTE*, *Swift*) permitted it to be classified as a low-mass X-ray binary, which was probably hosting a black hole (e.g. Lutovinov et al. 2005; Capitanio et al. 2009). The renewal of activity in late January 2011 (Krimm et al. 2011; Krimm & Kennea 2011) prompted several observing campaigns on the source. It was, in particular, found that IGR J17091–3624 has similarities with GRS

Send offprint requests to: J. Rodriguez: jrodriguez@cea.fr

arXiv:1108.0666v1 [astro-ph.HE] 2 Aug 2011

1915+105, since it showed types of X-ray variability reminiscent of those of the so-called “ ρ -heartbeat” and “ β ” classes seen in GRS 1915+105 (Altamirano et al. 2011a,b). The specifics of the IGR J17091–3624’s X-ray behaviour further justify a (simultaneous) multi-wavelength study, to see, in particular, how it compares to the other ~ 17 BHBs with known radio-X-ray behaviour.

Early in the outburst, we reported the presence of radio emission compatible with a compact jet in the HS (Corbel et al. 2011) and a ~ 0.1 Hz QPO at the same time (Rodríguez et al. 2011). Here, we present an in-depth analysis of four (quasi) simultaneous radio-X-ray observations. To complement the *ATCA* and *RXTE* data, we use *INTEGRAL* and *Swift* observations to enhance the spectral coverage.

Table 1. Radio fluxes of IGR J17091–3624 during the four *ATCA* observations. Errors are at the 1σ level.

| Obs. | $F_{5.5\text{GHz}}$ (mJy) | $F_{9\text{GHz}}$ (mJy) | α |
|------|------------------------------|----------------------------|------------------|
| A1 | 1.40 \pm 0.05 | 1.24 \pm 0.06 | -0.25 \pm 0.12 |
| A2 | 1.53 \pm 0.10 | 1.57 \pm 0.10 | +0.05 \pm 0.19 |
| A3 | 2.41 \pm 0.10 | 1.13 \pm 0.10 | -1.54 \pm 0.20 |
| A4 | 0.17 \pm 0.05 | <0.08 | |

2. Observations and data reduction

Figure 1 shows the 15–50 keV daily averaged *Swift*/BAT lightcurve of IGR J17091–3624, with the various observations discussed in this paper. The journal of these observations can be found online in Table 4. The observations are, hereafter, ordered and labelled according to the instrument used (A stands for *ATCA*, I for *INTEGRAL*, S for *Swift*, and R for *RXTE*). The *ATCA* observations were made in two frequency bands (5.5 and 9 GHz) simultaneously, with the upgraded Compact Array Broadband Backend (Wilson et al. 2011). The amplitude and band-pass calibrator was PKS 1934–638, and the antenna’s gain and phase calibration, as well as the polarisation leakage, were derived from regular observations of the nearby ($\sim 3.2^\circ$ away) calibrator PMN 1714–336. See, e.g., Corbel et al. (2004) for more details on the standard data reduction.

The *RXTE* and *Swift* data were reduced with HEASOFT¹ v6.10, and the *INTEGRAL* data with OSA v9.0². The X-ray spectral fitting software package XSPEC 12.6.0q was used to fit the energy and power density spectra (PDS) after converting the latter into XSPEC readable files.

The *Swift*/XRT level 2 cleaned event files were obtained from window timing (WT) mode data with xrtpipeline keeping only the grade 0 events. We then extracted the spectra from a 40×10 pixel region centred on the best source position. The background was estimated from a region of the same size at an off-axis position. The ancillary response file (arf) was estimated with xrtrmkarf, and the last version (v. 12) of the WT redistribution matrix file (rmf) was used in the spectral fits.

The *INTEGRAL*/IBIS/ISGRI source spectra were obtained in a standard way (e.g. Rodríguez et al. 2008a). We used the latest version of the rmf and arf files available from the *INTEGRAL* instrument calibration tree provided with OSA 9.0. In two observations, the source is also within the field of view (fov) of the JEM-X monitors, and we extracted 16 channels spectra from JEM-X unit 2.

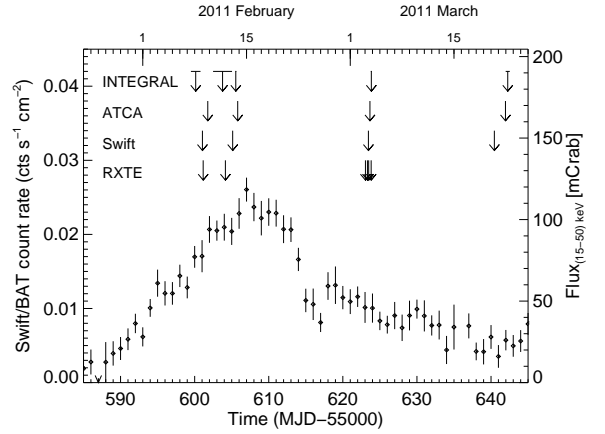


Fig. 1. 15–50 keV *Swift*/BAT lightcurve of IGR J17091–3624. The vertical arrows represent the (mid) times of the pointed observations. The width of the arrow’s top is the length of the observation (visible only for *INTEGRAL*).

The Z source GX 349+2 is at $\sim 41'$ from IGR J17091–3624. The *RXTE*/PCA data are thus contaminated by the emission from this bright source at a level that is very difficult to estimate given the lack of strictly simultaneous data. The *RXTE*/PCA data were therefore only considered for timing analysis (e.g. Rodríguez et al. 2011). Two to 60 keV PDS were extracted from Good Xenon mode data with POWSPEC v1.0 over the 0.0078125–500 Hz range. The fits of these PDSs were restricted to the frequency range 0.0078125–30 Hz.

3. Results

3.1. Radio observations

The analysis of the *ATCA* data shows there is a single radio source within the X-ray error circle, at a location of $(\alpha, \delta) = 17^{\text{h}} 09^{\text{m}} 07^{\text{s}}.61, -36^\circ 24' 25''.7$ (J2000, 1σ positional uncertainty of $0.1''$). This position is also consistent with the position of the suggested optical/NIR counterpart (Torres et al. 2011). The measured radio fluxes and spectral indices α (defined by $F(\nu) \propto \nu^\alpha$) are reported in Table 1.

3.2. X and γ -ray spectral analysis

The *Swift* and *INTEGRAL* spectra S1+I1, S2+I2, S3+I3, and S4+I4 were fitted simultaneously, and we retained the energy channels 0.7–7.5 keV for XRT, 20–300 keV for ISGRI, and, in S1+I1 and I1', the 4–20 keV channels for JEM-X2. The best-fit models consist of an absorbed³ power law with a high energy cut-off (tbabs*cutoffpl in XSPEC, hereafter CPL) for spectra S1+I1, I1', and S2+I2. A disc component is required in S3+I3 and S4+I4, while the cut-off is not needed any more (tbabs*(diskbb+powerlaw), hereafter DPL). A normalisation constant was also included and frozen to 1 for the XRT spectra and left free to vary for the other instruments, except for the I1' fits, where it is frozen to 1 for ISGRI. The best-fit parameters we obtained are reported in Table 2, and the ' ν - F_ν ' spectra of S1+I1 and S3+I3 are represented in Fig. 2.

In XRBs, a cut-off power-law spectrum is usually interpreted as the signature of inverse Comptonisation of soft seed

¹ <http://heasarc.gsfc.nasa.gov/docs/software/lheasoft/>

² <http://www.isdc.unige.ch/integral/analysis#Software>

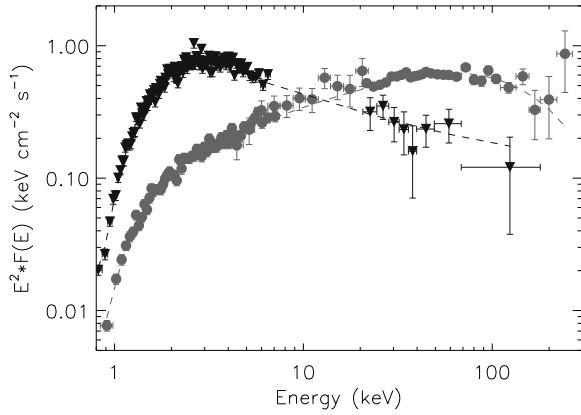
³ Abundances fixed to those from Wilms et al. (2000)

Table 2. Results of the spectral fits to the joint *Swift*/XRT and *INTEGRAL*/ISGRI (and JEM-X in I1 and I1') spectra. Errors are at the 90% level.

| Spectra | model | N_{H} ($\times 10^{22}$ cm $^{-2}$) | $kT_{\text{bb}}/kT_{\text{inj}}$ (keV) | Γ/τ | E_{cut}/kT_e (keV) | χ^2_{dof} | Unabs. Flux* | | |
|------------------|-------|---|---|---------------------|--------------------------------|-----------------------|--------------|---------|------------|
| | | | | | | | 0.5–10 keV | 3–9 keV | 20–200 keV |
| S1+I1 | CPL | 1.08 ± 0.08 | | 1.40 ± 0.07 | 100^{+17}_{-13} | 0.90 (89) | 8.4 | 4.5 | 20.0 |
| | ThC | $1.14^{+0.06}_{-0.05}$ | 0.2 (frozen) | 0.8 ± 0.3 | 85^{+43}_{-22} | 1.00 (89) | 8.5 | 4.3 | 17.2 |
| I1' | CPL | 1.1 frozen | | 1.49 ± 0.09 | 91^{+17}_{-13} | 1.0 (34) | NA | 6.5 | 22.4 |
| | ThC | 1.1 frozen | 0.2 (frozen) | 0.8 ± 0.2 | 74^{+22}_{-10} | 1.0 (34) | NA | 7.2 | 22.3 |
| S2+I2 | CPL | 1.15 ± 0.06 | | 1.54 ± 0.05 | 107^{+61}_{-32} | 1.1 (137) | 12.1 | 6.0 | 20.8 |
| | ThC | 1.13 ± 0.05 | 0.2 (frozen) | $2.1^{+0.5}_{-1.5}$ | 27^{+74}_{-7} | 1.2 (137) | 11.7 | 6.0 | 25.9 |
| S3+I3 | DPL | 1.5 ± 0.1 | 1.2 ± 0.2 | 2.3 ± 0.3 | | 1.3 (128) | 38.2 | 11.4 | 7.3 |
| S4+I4 $^{\circ}$ | DPL | 1.16 ± 0.05 | $1.29^{+0.01}_{-0.03}$ | $2.1^{+0.1}_{-0.3}$ | | 1.2 (409) | 31.6 | 12.4 | 2.1 |

* In units of 10^{-10} erg cm $^{-2}$ s $^{-1}$. Fluxes are normalised to *Swift*/XRT, except I1' normalised to ISGRI

$^{\circ}$ Observations made more than a day apart. Norm. constant is high and poorly constrained (≥ 2).


Fig. 2. Spectra of obs. S1+I1 (XRT/JEM-X 2/ISGRI, grey filled circles) and S3+I3 (XRT/ISGRI, dark triangles). The dashed lines represent the best-fit models.

photons by a thermalised (i.e., with velocities following a Maxwellian distribution) population of electrons. A thermal Comptonisation model (comptt Titarchuk 1994) provided a good fit to S1+I1, I1', and S2+I2 (ThC in Table 2). We assumed a disc geometry in XSPEC and fixed the temperature of the seed photons. This model also permits avoiding the divergence of the power-law flux towards low energy since Comptonisation significantly contributes above $3 \times kT_{\text{inj}}$ and decreases quickly below.

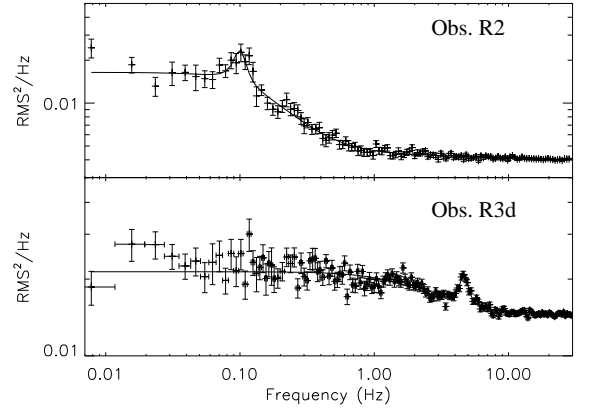
3.3. X-ray timing analysis

None of the *RXTE* observations shows the “ ρ -heartbeat” type of variability. Since GX 349+2 contaminates significantly Obs. R1 and R2 (Sec. 2), we do not discuss the level of continuum variability since we cannot attribute it to IGR J17091–3624 with certainty. The IGR J17091–3624 PDSs, however, show QPOs that are not associated with GX 349+2 (Rodríguez et al. 2011; Shaposhnikov 2011; Pahari et al. 2011). To obtain their ‘true’ amplitudes during Obs. R1 and R2, we have estimated the net count rate of IGR J17091–3624 in the *RXTE*/PCA by using our spectral results (Table 2) and simulated a PCA spectrum in XSPEC. The amplitude of the QPO is then $A_{\text{net}} = A_{\text{raw}} \times \frac{CR_{\text{PCA}}}{CR_{\text{net}}}$, where A_{raw} is the rms amplitude of the QPO obtained from the fit to the PDS, CR_{net} the simulated count rate of IGR J17091–3624, and CR_{PCA} the observed PCA rate. No correction was applied to

R3a,b,c,d since GX 349+2 was out of the PCA fov. The QPO parameters obtained from the analysis are reported in Table 3, and two representative PDSs are plotted in Fig. 3. These QPOs can be classified as type C QPOs, except maybe those found in observations R3 that could be transitory between C and B.

Table 3. Parameters of the QPOs seen during Obs. R1, R2, and R3. Errors are given at the 90% confidence level.

| PDS | ν_{QPO} (Hz) | Q ($=\nu/\text{FWHM}$) | A (% rms) |
|-----|----------------------------|-----------------------------|----------------------|
| R1 | $0.081^{+0.005}_{-0.004}$ | 4.3 ± 2.2 | $12.3^{+1.8}_{-1.7}$ |
| R2 | $0.100^{+0.008}_{-0.005}$ | 4.2 ± 1.5 | $10.1^{+1.2}_{-1.6}$ |
| R3a | 4.57 ± 0.08 | 4.2 ± 1.1 | 8.8 ± 1.2 |
| R3b | 4.57 ± 0.08 | 4.5 ± 1.3 | $8.5^{+1.1}_{-1.3}$ |
| R3c | 4.28 ± 0.06 | 2.4 ± 0.3 | $12.5^{+0.5}_{-0.7}$ |
| R3d | 4.66 ± 0.05 | 5.8 ± 1.5 | 8.0 ± 0.6 |


Fig. 3. PDSs of observations R2 (top panel) and R3d (bottom panel).

4. Discussion

In the first two observations, the spectral parameters (Table 2) and presence of type C QPOs are typical of a BH in the HS (e.g. Remillard & McClintock 2006; Homan et al. 2005). During the third observation, the source clearly is in a softer state. The transition is associated with a discrete radio ejection (see below) as often seen in BHs (the clearest example being GRS 1915+105, e.g. Rodríguez et al. 2008a). This, and the presence of QPOs at

4–5 Hz, indicates that IGR J17091–3624 is in a SIMS at that time. No temporal (*RXTE*) data are available for the fourth observation. The spectra are indicative of either a SIMS or a pure SS.

The value of N_{H} obtained from the spectral fits is slightly higher than the $2^\circ \times 2^\circ$ weighted averaged absorption in this direction ($N_{\text{H}} = 6.0 \times 10^{21} \text{ cm}^{-2}$; Kalberla et al. 2005). This is consistent with a source lying at a rather large distance in the Galaxy.

The HS→SIMS state transition occurred between MJDs 55612 and 55616 (Pahari et al. 2011). Obs. 2 is the observation in the HS that is the closest to the peak of the hard X-ray outburst (Fig. 1) and to the state transition. It has a bolometric flux of $F_{\text{bol,trans}} \sim 4.1 \times 10^{-9} \text{ erg cm}^{-2} \text{ s}^{-1}$ (ThC model). Most BHBs have $L_{\text{trans,HS} \rightarrow \text{SS}} \gtrsim 4\% L_{\text{Edd},1-200\text{keV}}$, when assuming a power-law spectrum with $\Gamma=2$ (Yu & Yan 2009)⁴. Although this value slightly underestimates the bolometric luminosity at the transition, we take it as a ‘hard’ lower limit on L_{trans} , which therefore allows us to estimate a lower limit on the distance to the source. Using $F_{\text{bol,trans}}$ estimated above, we obtain a distance $d_{\text{J17091}} \sim 11 \text{ kpc}$ for a BH of $\sim 10 M_{\odot}$. With $L_{\text{trans}} = 10\% L_{\text{Edd}}$ (Esin et al. 1997) we obtain $d_{\text{J17091}} \sim 17 \text{ kpc}$ ⁵. Using a different method (based on the QPO frequency–photon index correlation), Pahari et al. (2011) also favour a large distance with a range of masses between 8–11.4 M_{\odot} .

The radio spectra of observations A1 and A2 are consistent with being flat and they indicate of the presence of self-absorbed compact jets (e.g. Corbel et al. 2004; Fender et al. 2004). Observations A3 and A4 are characteristic of optically thin synchrotron emission and can be attributed to the emission of a discrete ejection associated with the hard to soft transition. The observation of yet another BHB showing discrete ejections at the hard to soft transition probably indicates a link between transitions and (discrete) ejections potentially common to all microquasars. In XTE J1550–564 and GRS 1915+105, Rodríguez et al. (2003, 2008a,b) have suggested that the Comptonised component was the source of the ejected material. Here, the change in spectral shape and drop in the hard X-ray flux (Table 2) is compatible with this interpretation.

In Fig. 4, we plot the levels of radio and X-ray emission for IGR J17091–3624 in comparison with a sample of representative BHBs (data from Corbel et al. 2003, 2008; Coriat et al. 2011; Rushton et al. 2010) assuming the distances estimated above. The two radio points with the lowest X-ray luminosities correspond to the HS, while the other two correspond to the optically thin radio flare. At a distance of 11 kpc, the source behaviour joins the track followed by H1743–322 (Fig. 4). In this case (and at any lower distance), however, the break of the radio vs X-ray relation occurs at too low luminosities compared to the standard BHBs (Fender et al. 2010). At 17 kpc the position of IGR J17091–3624 is consistent with the radio/X-ray correlation of most BHBs (within the dispersion), although we cannot assign it precisely to a specific track (i.e. the GX 339–4 or the H 1743–322 one, Fig. 4). In any cases, a large distance ($\gtrsim 11 \text{ kpc}$) to the source is favoured by the radio-X-ray behaviour.

IGR J17091–3624 has recently been compared to GRS 1915+105 (Altamirano et al. 2011a,b; Pahari et al. 2011). However, even at the favoured distance of 17 kpc, our simultaneous radio-X-ray observations show that IGR J17091–3624

does not reach the bright levels of radio luminosity observed for GRS 1915+105 (Fig. 4), and is more similar to standard BHBs, such as GX 339–4 or H1743–322. This would tend to indicate that the radio properties discussed here are not related to the fast flaring X-ray behaviour common to both GRS 1915+105 and IGR J17091–3624.

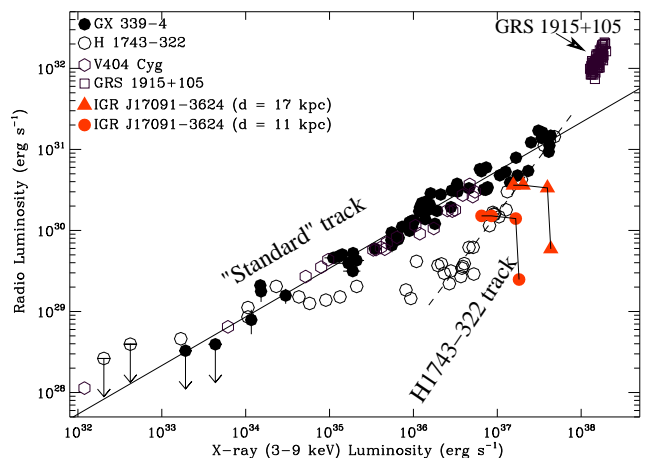


Fig. 4. Radio vs X-ray luminosity for several BHBs.

Acknowledgements. We thank P. Varnière, R. Owen, and P. Curran for useful discussions. JR and SC acknowledge partial funding from the European FP7 grant agreement number ITN 215212 “Black Hole Universe”. IC is supported by the CNES through CNRS. JAT acknowledges partial support from NASA via INTEGRAL and Swift Guest Observer grants NNX08AX93G and NNX08AW35G. AP acknowledges financial contribution from the agreement ASI-INAF I/009/10/0. The Australia Telescope is funded by the Commonwealth of Australia for operation as a national facility managed by CSIRO. We acknowledge the use of the IGR Sources page (<http://irfu.cea.fr/Sap/IGR-Sources/>), the use of public *Swift* and *RXTE* data obtained through the HEASARC Online Service, provided by NASA/GSFC, and observations made with *INTEGRAL*, an ESA project with instruments and science data centre funded by ESA member states, Poland and with the participation of Russia and the USA.

References

- Altamirano, D., et al. 2011a, *The Astronomer’s Telegram*, 3299, 1
 Altamirano, D., et al. 2011b, *The Astronomer’s Telegram*, 3225, 1
 Capitanio, F., Giroletti, M., Molina, M., et al. 2009, *ApJ*, 690, 1621
 Corbel, S., Fender, R. P., Tomsick, J. A., Tzioumis, A. K., & Tingay, S. 2004, *ApJ*, 617, 1272
 Corbel, S., Koerding, E., & Kaaret, P. 2008, *MNRAS*, 389, 1697
 Corbel, S., Nowak, M. A., Fender, R. P., Tzioumis, A. K., & Markoff, S. 2003, *A&A*, 400, 1007
 Corbel, S., et al. 2011, *The Astronomer’s Telegram*, 3167, 1
 Coriat, M., Corbel, S., Prat, L., et al. 2011, *MNRAS*, 619
 Esin, A. A., McClintock, J. E., & Narayan, R. 1997, *ApJ*, 489, 865
 Fender, R. 2006, *Jets from X-ray binaries (Compact stellar X-ray sources)*, 381–419
 Fender, R. P., Belloni, T. M., & Gallo, E. 2004, *MNRAS*, 355, 1105
 Fender, R. P., Gallo, E., & Russell, D. 2010, *MNRAS*, 406, 1425
 Homan, J., Buxton, M., Markoff, S., et al. 2005, *ApJ*, 624, 295
 Kalberla, P. M. W., Burton, W. B., Hartmann, D., et al. 2005, *A&A*, 440, 775
 Krimm, H. A., et al. 2011, *The Astronomer’s Telegram*, 3144, 1
 Krimm, H. A. & Kennea, J. A. 2011, *The Astronomer’s Telegram*, 3148, 1
 Kuulkers, E., et al. 2003, *The Astronomer’s Telegram*, 149, 1
 Laurent, P., Rodríguez, J., Wilms, J., et al. 2011, *Science*, 332, 438
 Lutovinov, A., Revnivtsev, M., Molkov, S., & Sunyaev, R. 2005, *A&A*, 430, 997
 Pahari, M., Yadav, J., & Bhattacharyya, S. 2011, submitted, *ArXiv* 1105.4694
 Remillard, R. A. & McClintock, J. E. 2006, *ARA&A*, 44, 49
 Remillard, R. A., Sobczak, G. J., Munro, M. P., & McClintock, J. E. 2002, *ApJ*, 564, 962
 Rodríguez, J., Corbel, S., & Tomsick, J. A. 2003, *ApJ*, 595, 1032
 Rodríguez, J., et al. 2011, *The Astronomer’s Telegram*, 3168, 1

⁴ With exception of Cyg X-1 (HMXB) and GRO J1655–40 (discussed as an outlier by Yu & Yan 2009).

⁵ Fit of non simultaneous *Swift*/*INTEGRAL* observations performed on MJDs 55611–55612 leads to $F_{\text{bol,trans}} \sim 3.5 \times 10^{-9} \text{ erg cm}^{-2} \text{ s}^{-1}$. This lower value would place IGR J17091–3624 at an even farther distance.

- Rodriguez, J., Hannikainen, D. C., Shaw, S. E., et al. 2008a, *ApJ*, 675, 1436
Rodriguez, J., Shaw, S. E., Hannikainen, D. C., et al. 2008b, *ApJ*, 675, 1449
Rushton, A., Spencer, R., Fender, R., & Pooley, G. 2010, *A&A*, 524, A29+
Shaposhnikov, N. 2011, *The Astronomer's Telegram*, 3179, 1
Titarchuk, L. 1994, *ApJ*, 434, 570
Torres, M. A. P., et al. 2011, *The Astronomer's Telegram*, 3150, 1
Wilms, J., Allen, A., & McCray, R. 2000, *ApJ*, 542, 914
Wilson, W. E., Ferris, R. H., Axtens, P., et al. 2011, *ArXiv* 1105.3532
Yu, W. & Yan, Z. 2009, *ApJ*, 701, 1940

Table 4. Journal of the multi-wavelength observations of IGR J17091–3624 presented in this paper.

| Facility | label | Obs. Id (when available) | MJD start (d) | Good time |
|-----------------|-----------------|-----------------------------|------------------|-----------|
| <i>ATCA</i> | A1 | | 55601.64 | 3.1 h |
| | A2 | | 55605.73 | 1.9 h |
| | A3 | | 55623.57 | 2.2 h |
| | A4 | | 55641.85 | 2.4 h |
| <i>RXTE</i> | R1 | 96103-01-01-00 | 55601.15 | 2486 s |
| | R2 | 96103-01-02-00 | 55604.15 | 5668 s |
| | R3a | 96420-01-01-010 | 55623.05 | 6755 s |
| | R3b | 96420-01-01-01 | 55623.32 | 4695 s |
| | R3c | 96420-01-01-020 | 55623.49 | 16263 s |
| <i>Swift</i> | R3d | 96420-01-01-02 | 55623.82 | 7834 s |
| | S1 | 00031921005 | 55601.05 | 1457 s |
| | S2 | 00031921009 | 55605.13 | 2167 s |
| | S3 | 00031921019 | 55623.45 | 686 s |
| <i>INTEGRAL</i> | S4 | 00031921030 | 55640.45 | 2352 s |
| | I1 | Rev 1016* | 55599.49 | 61080 s |
| | I1 [†] | Rev 1017 | 55602.49 | 131000 s |
| | I2 | Rev 1018 | 55605.48 | 7818 s |
| | I3 | Rev 1024 | 55623.77 | 6417 s |
| | I4 | Rev 1030 | 55641.98 | 8583 s |

* *INTEGRAL* revolution number.† I1[†] is intermediate (in time) between Obs. I1 and Obs. I2.